Biophysical Chemistry 26 (1987) 337–355
Elsevier



BPC 01150

# Rebinding and relaxation in the myoglobin pocket

Anjum Ansari, Joel Berendzen, David Braunstein, Benjamin R. Cowen, Hans Frauenfelder, Mi Kyung Hong, Icko E.T. Iben, J. Bruce Johnson, Pál Ormos *, Todd B. Sauke, Reinhard Scholl, Alfons Schulte, Peter J. Steinbach, Joseph Vittitow and Robert D. Young **

*Departments of Physics and Biophysics, University of Illinois at Urbana-Champaign, Urbana, IL 61801, U.S.A.*

Accepted 27 February 1987

Myoglobin; CO stretching band; Conformational substate hierarchy; Protein relaxation; Protein dynamics; Control mechanism

The infrared stretching bands of carboxymyoglobin (MbCO) and the rebinding of CO to Mb after photodissociation have been studied in the temperature range 10–300 K in a variety of solvents. Four stretching bands imply that MbCO can exist in four substates, $A_0$ $A_3$. The temperature dependences of the intensities of the four bands yield the relative binding enthalpies and entropies. The integrated absorbances and pH dependences of the bands permit identification of the substates with the conformations observed in the X-ray data (Kuriyan et al., J. Mol. Biol. 192 (1986) 133). At low pH, $A_0$ is hydrogen-bonded to His E7. The substates $A_0$–$A_3$ interconvert above about 180 K in a 75% glycerol/water solvent and above 270 K in buffered water. No major interconversion is seen at any temperature if MbCO is embedded in a solid polyvinyl alcohol matrix. The dependence of the transition on solvent characteristics is explained as a slaved glass transition. After photodissociation at low temperature the CO is in the heme pocket B. The resulting CO stretching bands which are identified as B substates are blue-shifted from those of the A substates. At 40 K, rebinding after flash photolysis has been studied in the Soret, the near-infrared, and the integrated A and B substates. All data lie on the same rebinding curve and demonstrate that rebinding is nonexponential in time from at least 100 ns to 100 ks. No evidence for discrete exponentials is found. Flash photolysis with monitoring in the infrared region shows four different pathways within the pocket B to the bound substates $A_i$. Rebinding in each of the four pathways B → A is nonexponential in time to at least 10 ks and the four pathways have different kinetics below 180 K. From the time and temperature dependence of the rebinding, activation enthalpy distributions $g(H_{BA})$ and preexponentials $A_{BA}$ are extracted. No pumping from one A substate to another, or one B substate to another, is observed below the transition temperature of about 180 K. If MbCO is exposed to intense white light for $10$–$10^3$ s before being fully photolyzed by a laser flash, the amplitude of the long-lived states increases. The effect is explained in terms of a hierarchy of substates and substate symmetry breaking. The characteristics of the CO stretching bands and of the rebinding processes in the heme pocket depend strongly on the external parameters of solvent, pH and pressure. This sensitivity suggests possible control mechanisms for protein reactions.

## 1. Introduction

The binding of small ligands such as carbon monoxide (CO) to heme proteins at first appears to be a simple one-step process [1], but a closer look over extended ranges in temperature, time, and wavelength reveals a surprising complexity. Binding is governed by a sequence of barriers rather than a single one [2]. After photodissociation, rebinding occurs at temperatures as low as a

Dedicated to Professor Manfred Eigen on the occasion of his 60th Birthday.

Correspondence address: H. Frauenfelder, Department of Physics, 1110 W. Green St., University of Illinois at Urbana-Champaign, Urbana, IL 61801, U.S.A.

* Permanent address: Institute of Biophysics, Biological Research Center, Hungarian Academy of Sciences, Szeged H-6701, Hungary.

** Permanent address: Department of Physics, Illinois State University, Normal, IL 61761, U.S.A.

few Kelvin [3] and is nonexponential in time below 180 K in a 75% glycerol/water solvent [2,4,5]. Below about 40 K, binding no longer proceeds by classical over-the-barrier motion, but through quantum-mechanical tunneling [6,7]. The behavior of the photodissociated CO within the heme pocket, followed by infrared spectroscopy, turns out to be complicated [8,9].

In the present paper we investigate processes within the heme pocket of myoglobin (Mb) in more detail. Mb has been called the hydrogen atom of biology; it is a globular protein of about 18 kDa that stores dioxygen ($O_2$) in muscles [10]. $O_2$ or CO binds reversibly to the central iron atom of the heme group in Mb. Since Mb is sturdy and has been very well explored, it offers a nearly ideal system for more sophisticated studies.

The impetus for the present work came from two directions: (1) At low temperatures, CO bound to Mb shows a number of stretching bands [8,9]. During our earlier work we had noticed that the different bands rebind with different rates after photodissociation. A rate difference has also been noticed by Gerwert et al. [11] and M. Chance et al. [12]. Such a rate variation suggests a control mechanism and calls for more studies. (2) Nonexponential kinetics below 180 K has been seen in all protein-ligand systems that have been studied. In general, nonexponential time dependences can be explained by either homogeneous or inhomogeneous processes. By using a sequence of laser flashes repeated before all of the Mb molecules have rebound a CO ('hole burning in time') we have demonstrated that pumping from short-lived to long-lived states at 60 and 70 K is very small and that the nonexponential kinetics results predominantly from inhomogeneities among Mb molecules and cannot be explained by multiple states within one protein molecule [5,13,14]. In view of these results it is surprising that B. Chance et al. recently claimed evidence for a bi- or triexponential time course and considerable pumping from short- to long-lived components in the binding of CO to Mb at 40 K [15]. The difference between their interpretation and ours is fundamental. B. Chance et al. assume that the different lifetimes are caused by different pathways or sites within the same molecule. We postulate a large number of structurally different conformational substates (CS), with each molecule remaining in a given CS at temperatures where the solvent is frozen [5,16]. Our interpretation leads to the concept of a hierarchy of substates [17] and to connections between proteins and (spin) glasses [18]. We will discuss the concept of CS and of the hierarchy of CS in section 4.5.

Here we report on expanded low-temperature experiments [19]. The new experiments verify our earlier experiments and also yield surprising results that open new windows on phenomena in the heme pocket.

## 2. Experimental approach

The primary experimental technique is low-temperature flash photolysis. An MbCO sample at a controlled temperature is photodissociated with a light pulse and rebinding is monitored through optical absorption measurements. We have observed rebinding at many different wavelengths, as indicated in fig. 1, thus monitoring the rebinding process(es) at different locations in the heme pocket [20,21]. In the Soret and the $\alpha$- and $\beta$-bands, changes in the electronic structure of the heme on binding are seen. The near-infrared band (band III, near 760 nm) is a charge-transfer band and involves both the iron atom and the heme. In the infrared, the bands near 1950 $cm^{-1}$ result from the stretching mode of the bound CO [22,23] and those near 2100 $cm^{-1}$ from the stretching mode of the photodissociated CO within the pocket [8,9]. If only one simple rebinding process were to occur, all of these markers would give the same time course.

Four different systems were used for the experiments, a nanosecond visible-wavelength flash photolysis system, a conventional dispersive visible-near-infrared spectrometer, a Fourier transform infrared (FTIR) spectrometer and a microsecond mid-infrared flash photolysis system. Samples were prepared from lyophilized sperm whale Mb from Sigma (St. Louis, MO) dissolved in buffer solution. 0.4 M citrate-phosphate buffer was used for the pH 5.0 samples, 0.4 M carbonate-bicarbonate buffer for the pH 9.0 samples, 0.1 M Hepes buffer

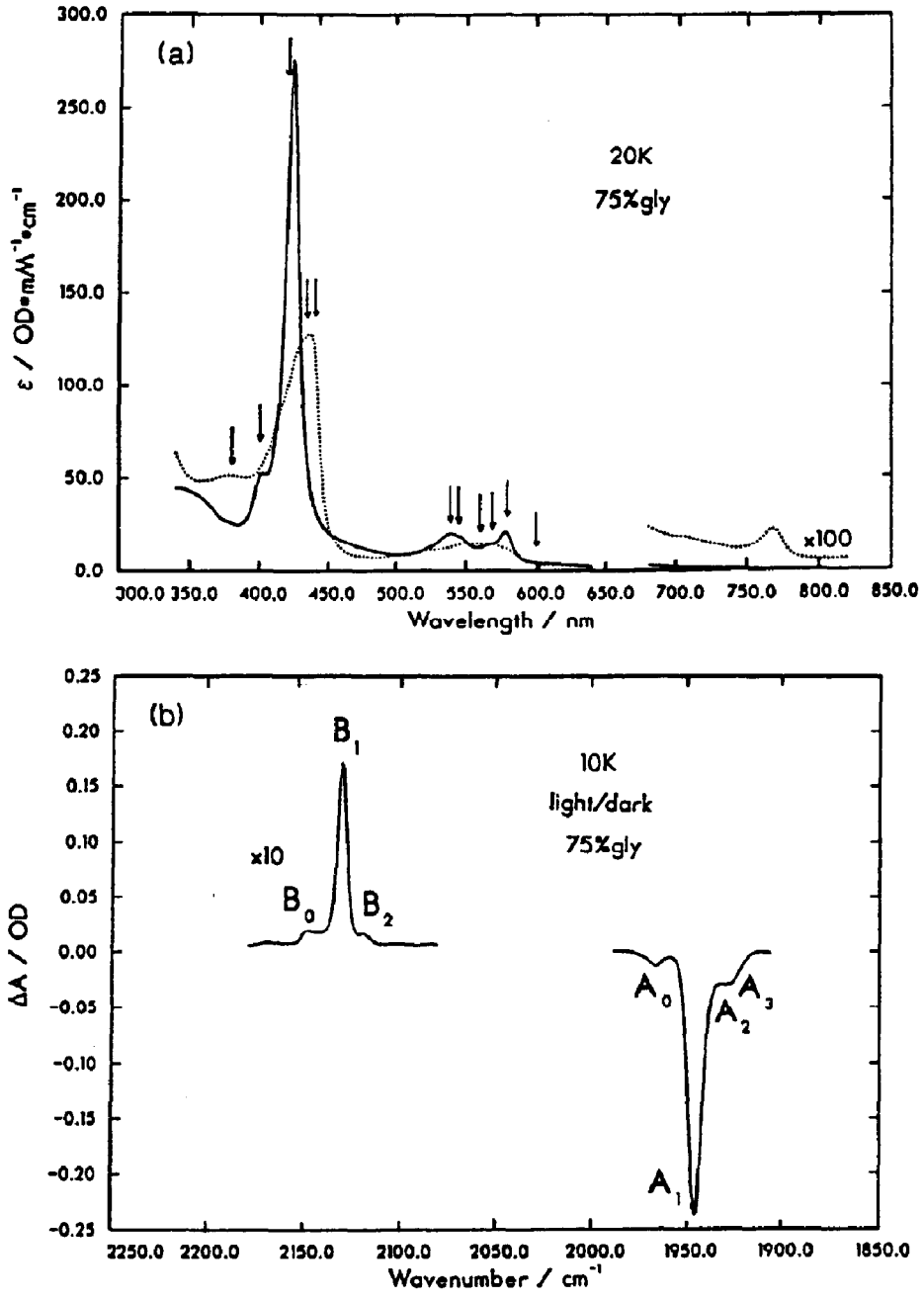


Fig. 1. The spectral range where rebinding is monitored. (a) Absorption spectra of Mb (· · · · ·) and MbCO (———) in the Soret, α- and β- and near-infrared regions. Arrows indicate where we have measured rebinding in the flash photolysis experiments. (b) Infrared difference spectrum (Mb − MbCO).

for the pH 7.0 polyvinyl alcohol (PVA) samples and 0.5 M sodium phosphate buffer for all of the other samples. Solvents used were water, 75% (v/v) glycerol/water, and PVA. The Soret data were taken on 10–14 $\mu$M samples placed in a $1 \times 1$ cm cuvette and the near-infrared experiments were performed on a 1.5 mM sample in a $1 \times 0.1$ cm cell [17]. FTIR and fast-infrared measurements were made on 15–20 mM samples held between two $CaF_2$ windows with a 75 $\mu$m mylar spacer.

The nanosecond system employed a 30 ns pulse from a frequency-doubled, Q-switched $Nd^+$-glass laser (530 nm, 300 mJ). Rebinding was monitored with the light from a tungsten lamp passed through a monochromator. Monitor beam intensities were kept small ($< 10^{-3}$ photons/s absorbed per protein molecule). The photomultiplier (Hamamatsu 928) signal was digitized with a LeCroy TR8818 transient digitizer from 10 ns to 300 $\mu$s and with a logarithmic time-base digitizer from 2 $\mu$s to 300 s. A storage cryostat (Janis 10-DT) permitted temperature control.

Our OLIS-Cary 14 spectrophotometer is interfaced to an IBM PC/AT computer. Kinetics data obtained from this instrument extend from 60 to $3 \times 10^4$ s.

The FTIR experiments were performed on a Mattson Sirius 100 FTIR spectrometer. All spectra were taken at 1 or 2 $cm^{-1}$ resolution. Low temperatures were produced with a closed-cycle helium refrigerator, CTI model 21. Photolysis in the kinetics experiments was achieved with two 500 ns, 0.3 J, 590 nm pulses, separated by approx. 1 s, from a Phase-R DL2100C dye laser using rhodamine 6G dye. Absolute absorbance spectra were obtained by subtracting the solvent background spectrum from the MbCO spectrum. The difference absorption spectra in the kinetics experiments were obtained by referencing the photolyzed spectrum to the unphotolyzed background spectrum.

The fast kinetics of the CO stretching bands was measured in a separate mid-infrared flash photolysis system. The infrared monitoring light was produced by a Spectra-Physics/Laser Analytics tunable-diode laser and directed through the protein solution and monochromator onto a liquid $N_2$-cooled IR-Associated HgCdTe detector. Photolysis was induced by a single pulse from the same laser used in the FTIR experiments. For times between 100 ms and 100 s the diode laser current was modulated at 10 kHz and the signal was amplified by a PAR 5101 lock-in amplifier.

## 3. Results and data evaluation

A coherent picture of the low-temperature binding emerges after the data obtained with the different instruments and in the different wavelength regions are pieced together.

### *3.1. Infrared measurements of MbCO*

#### *3.1.1. The A substates*

The stretching bands of the bound CO are superb probes. We have measured the 'dark' or bound-state infrared spectrum of MbCO at temperatures between 15 and 300 K in 75% glycerol/water (fig. 2), water (fig. 3), and solid PVA (fig. 4).

The spectra shown in figs. 2–4 can be decomposed into Gaussian superpositions of Lorentzians, called Voigtians [24,25]. Two such decompositions are shown in fig. 5. Four different infrared bands can be distinguished. We denote the bands in

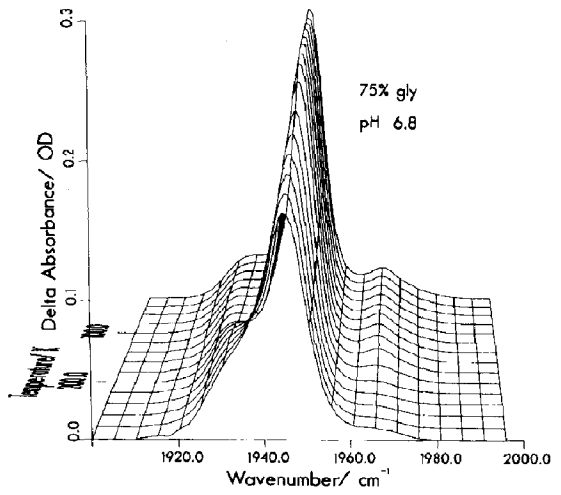


Fig. 2. Temperature-dependent infrared spectrum of the CO stretching bands of MbCO. Solvent: 75% glycerol/water, pH 6.8.

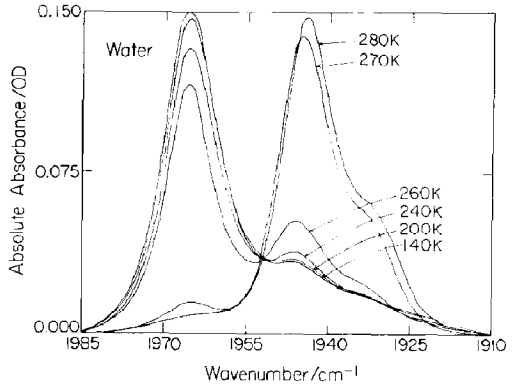


Fig. 3. Temperature-dependent spectrum of the CO stretching bands in MbCO. Solvent: water, pH 6.7.

order of decreasing wave numbers by $A_0$ ($\approx 1966$ cm$^{-1}$), $A_1$ ($\approx 1946$ cm$^{-1}$), $A_2$ ($\approx 1941$ cm$^{-1}$) and $A_3$ ($\approx 1930$ cm$^{-1}$). (Because of the new band $A_2$ the nomenclature differs from the one we used earlier [8]). The fits yield the center positions $\nu_{CO}$, the full-width at half-maximum $\Gamma$, and the areas of the four bands. Since the band $A_2$ is difficult to extract unambiguously, we shall discuss only the other three.

### 3.1.2. *Temperature dependence of the A bands*

In order to characterize the temperature dependence of the *individual bands* in glycerol/water,

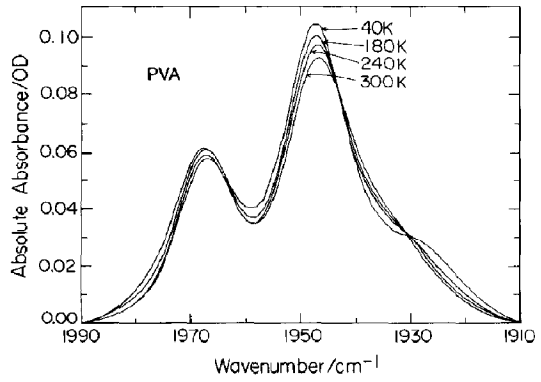


Fig. 4. Temperature-dependent spectrum of the CO stretching bands in MbCO. Solvent: solid PVA, pH 7.0.

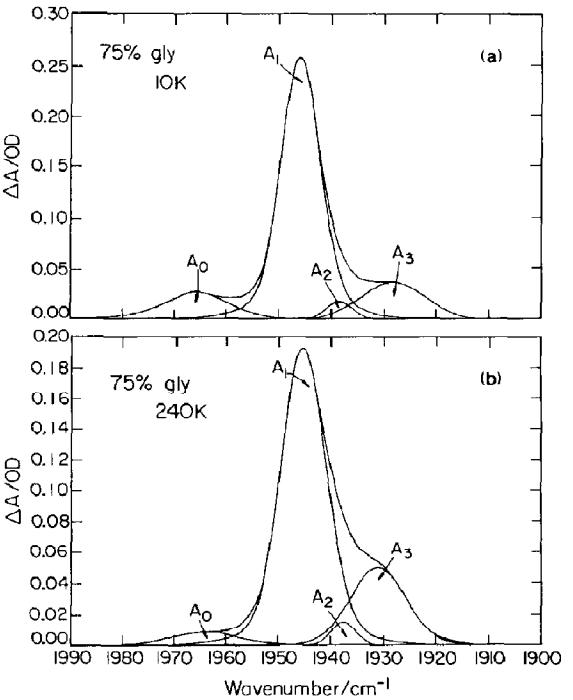


Fig. 5. Voigtian decomposition of the MbCO spectrum into four A substates at 10 and 240 K. Solvent: 75% glycerol/water, pH 6.8.

we select the most intense band, $A_1$, as standard and plot in fig. 6 the logarithm of the intensity ratios $A_0/A_1$ and $A_3/A_1$ as a function of $10^3/T$. The ratios $A_i/A_1$ in fig. 6 show a different behavior for PVA and glycerol/water. For PVA, the ratios change very little. MbCO in 75% glycerol/water, in contrast, shows two regions. Above about 180 K, the ratios change rapidly; below that temperature, the change is much slower. The behavior above 180 K can be understood if the four bound substates $A_0$–$A_3$ have different binding enthalpies and entropies and may interconvert freely. Below 180 K, the change may be explained by assuming that the proteins are frozen into particular substates and that the extinction coefficients for the different A substates depend slightly differently on temperature. Above 180 K, the ratios are given by

$$A_i/A_1 = \exp[S_i/R]\,\exp[-H_i/RT] \times \{\epsilon_i(T)/\epsilon_1(T)\} \qquad (1)$$

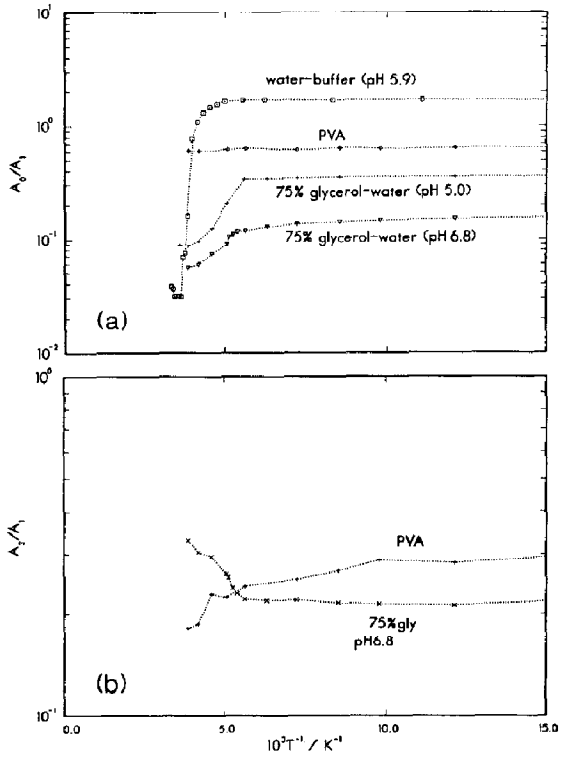


Fig. 6. Plots of (a) $(A_0/A_1)$ and (b) $A_3/A_1$ vs. $10^3/T$. $A_i/A_1$ is the ratio of the areas of the stretching bands in the bound states $A_i$ and $A_1$. Below 180 K, the ratios change little.

where $S_i$ and $H_i$ are the entropy and enthalpy of substate $A_i$ with respect to substate $A_1$ and $\epsilon_i(T)$ is the extinction coefficient of substate $A_i$ at temperature $T$. Assuming as a first approximation that the ratio of extinction coefficients is unity, relative binding enthalpies and entropies have been extracted from the data in fig. 6. The binding parameters for two values of pH are given in table 1.

The *total integrated area* $\Sigma A_i$ of the A bands of MbCO in 75% glycerol/water, given as a function of temperature in fig. 7, shows a decrease of about 20% in going from 10 to 300 K. Such a decrease can be explained by a change in the electron-nuclear coupling [26].

The temperature dependence of the *center frequency* $\nu_{CO}$ is given in fig. 8 for the bands $A_0$ and $A_1$ for two samples. The temperature dependence of the *linewidth* $\Gamma$ is displayed in fig. 9.

Table 1

Relative binding parameters of the A substates

$R$, gas constant; solvent, 75% glycerol/water.

| Substate | $H_A$ (kJ/mol) | | $S_A/R$ | |
|---|---|---|---|---|
| | pH 6.8 | pH 5.0 | pH 6.8 | pH 5.0 |
| $A_0$ | −4 | −8 | −5 | −7 |
| $A_1$ | 0 | 0 | 0 | 0 |
| $A_3$ | 2 | 2 | 0 | 0 |

*3.1.3. Nonequilibrium behavior of the A bands*

The ratios $A_0/A_1$ and $A_3/A_1$ in fig. 6 follow a van't Hoff behavior from 260 to 190 K. Below 190 K, they deviate from the van't Hoff line and become essentially temperature independent. We explain this temperature dependence by assuming that the A substates are not in dynamic equilibrium below about 180 K in 75% glycerol/water. To verify this assumption we have measured the time dependence of the infrared spectrum after the temperature was lowered from 195 K to the measurement temperature $T$. We denote with $A_i(t)$ the integrated absorbance of band $A_i$ at time $t$ after lowering the temperature. $A_i(0)$ is the integrated absorbance at 195 K, and $A_i(\infty)$ the equilibrium value at temperature $T$ which would

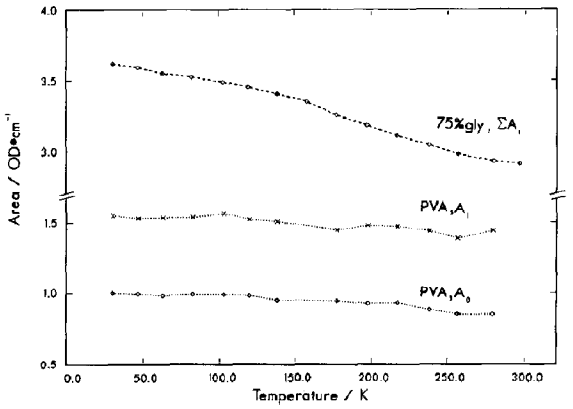


Fig. 7. Temperature-dependent area of the CO stretching bands in MbCO.

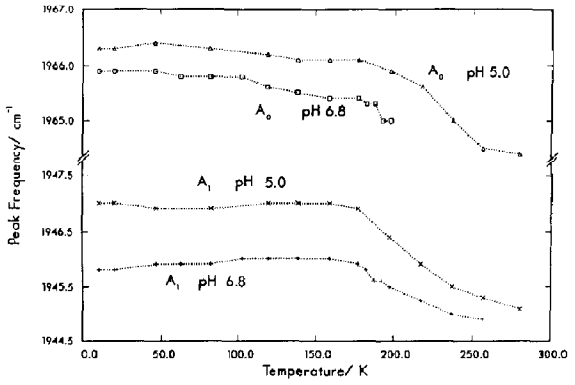


Fig. 8. Temperature dependence of the peak frequency of the CO stretching bands $A_0$ and $A_1$ in 75% glycerol/water at pH 5.0 and pH 6.8.

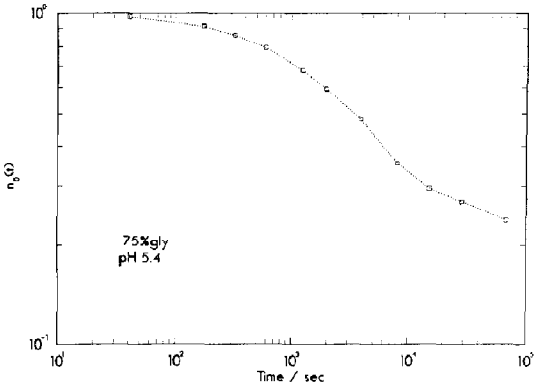


Fig. 10. Approach to equilibrium of substate $A_0$ after a change in temperature from 195 to 190 K. $n_0(t)$ denotes the fraction of MbCO that have not reached equilibrium in substate $A_0$ at time $t$ after the temperature change.

be reached after an extremely long (infinite) time. We estimate $A_i(\infty)$ by extrapolating the van't Hoff line, obtained from 260 to 195 K, to the temperature $T$. The fraction $n_i(t)$ of MbCO molecules that have not yet transferred to substate $A_i$ at time $t$ after the change in $T$ is given by

$$n_i(t) = \{A_i(t) - A_i(\infty)\}/\{A_i(0) - A_i(\infty)\}. \quad (2)$$

$n_0(t)$ at 190 K is shown in fig. 10. The data indicate that the approach to equilibrium is non-exponential in time. In addition, we observe that the time to reach equilibrium is extremely long below 180 K. The A substates are not in equilibrium below 180 K.

### 3.1.4. External influence on A substates

Makinen et al. [22] and Brown et al. [27] have pointed out that external influences can change the relative intensities of the A substates. Such effects can be seen in figs. 2–4. $A_0$ is much more intense in PVA and in ice than in glycerol/water. Pressure and pH also affect the ratio $A_i/A_1$. Fig. 11 shows that $A_3$ decreases while $A_1$ and $A_0$ increase with increasing pressure. Fig. 12 shows

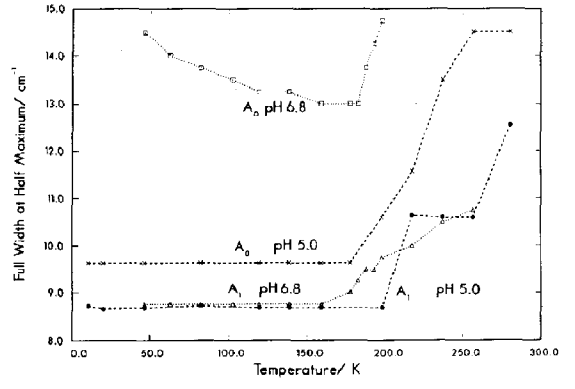


Fig. 9. Temperature dependence of the linewidths (full width at half maximum) of the A substates. Solvent: 75% glycerol/water, pH 6.8.

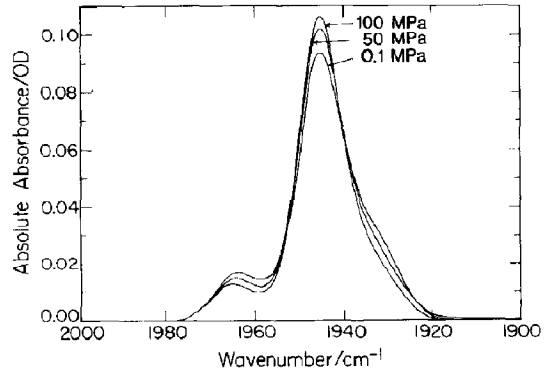


Fig. 11. The CO stretching bands of MbCO at 0.1, 50 and 100 MPa (1 MPa = 9.9 atm). Solvent: 75% glycerol/water, 0.25 M Tris-HCl buffer, pH 6.1.

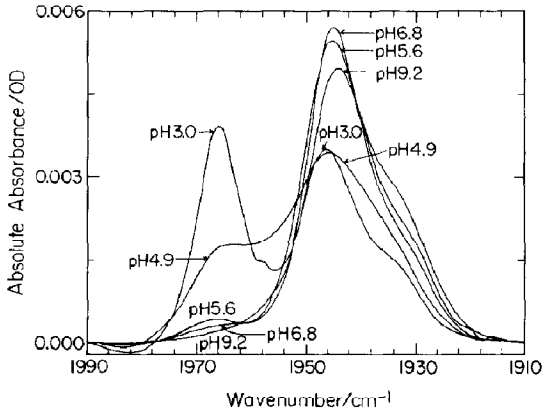


Fig. 12. The CO stretching bands of MbCO in 75% glycerol/water at various pH values.

that $A_0$ increases at the expense of $A_1$ with decreasing pH. While the band intensities are affected strongly by solvent state, pressure, and pH, the band positions remain nearly unchanged.

The close coupling of the environment with the protein is supported by the data in fig. 13. The infrared spectrum of a 75% glycerol/water solvent exhibits a transition near 180 K, essentially at the temperature where the substate exchange is frozen.

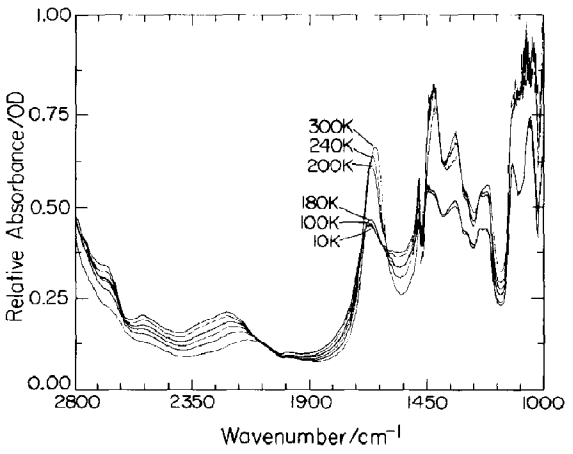


Fig. 13. Infrared spectrum of 75% glycerol/water solvent as a function of temperature.

### 3.2. Overall rebinding at 40 K

Fig. 1 shows that rebinding after photodissociation can be monitored at various locations in the heme-CO system. We have studied the rebinding at 40 K over a wide range of times at various wavelengths. We selected 40 K because B. Chance et al. [15] have claimed evidence for discrete exponentials at this temperature. The results of our measurements are shown in fig. 14. The data correspond to four different spectral regions. The symbol (◇) indicates measurement at 440 nm, near the deoxy Soret peak; (□) indicates the integrated absorbance of the '760 nm' charge-transfer band III; (▽) refers to the integral over all A (bound) CO stretching bands; and (○) shows the integrated magnitude of the absorbance change of the Soret band region from 400 to 450 nm.

The data in fig. 14 are smooth over more than 12 orders of magnitude in time. No evidence for the bi- or triexponential behavior is visible. Within experimental uncertainties all of the above measurements give the same time course.

### 3.3. Rebinding to the A substates

New features appear when the rebinding of each of the four A substates is monitored separately. Fig. 15 gives the rebinding of $A_0$, $A_1$ and

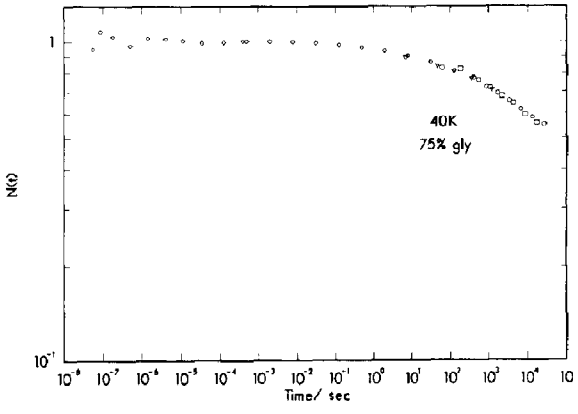


Fig. 14. Rebinding Mb + CO → MbCO at 40 K. (◇) 440 nm; (▽) integrated areas of the A bands; (○) integrated area in the Soret region, 400–450 nm; (□) integrated area of the 760 nm band. The individual rebinding curves have not been matched but have been normalized independently.

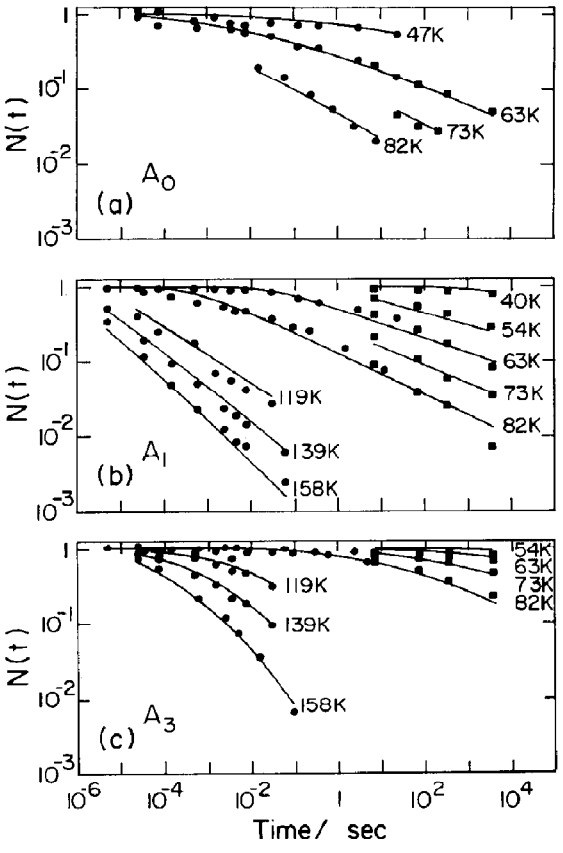


Fig. 15. Rebinding to the substate (a) $A_0$, (b) $A_1$, (c) $A_3$ as a function of time at various temperatures. (●) Mid-infrared flash photolysis data. (■) FTIR data. The solid lines are fits to the data using eqs. 3 and 4 and a gamma distribution for $g(H_{BA})$. The fit parameters $H_{peak}$ and $A_{BA}$ are listed in table 2. Solvent: 75% glycerol/water, pH 6.8.

$A_3$ at various temperatures. The data, taken at pH 6.8 in 75% glycerol/water, show the following features:

(a) At all temperatures, the four substates rebind with different kinetics.

(b) Rebinding of each A substate is nonexponential in time up to 180 K.

(c) $A_3$ is always considerably slower than $A_1$.

We evaluate the nonexponential kinetics by assuming that each protein molecule is in a substate with barrier height $H_{BA}$ for rebinding from the pocket state B to the covalently bound state A [5]. If $g(H_{BA})dH_{BA}$ denotes the probability of finding a barrier with height between $H_{BA}$ and $H_{BA} + dH_{BA}$, the rebinding function is given by

$$N(t) = N(0)\int dH_{BA}\, g(H_{BA})\, \exp[-k_{BA}(H_{BA})t], \quad (3)$$

Here $k_{BA}(H_{BA})$ is the rate coefficient appropriate for a barrier of height $H_{BA}$. Below about 40 K, $k_{BA}(H_{BA})$ is dominated by tunneling [6,7]. Above 40 K, $k_{BA}(H_{BA})$ is related to $H_{BA}$ by an Arrhenius relation,

$$k_{BA}(H_{BA}) = A_{BA}(T/T_0)\exp[-H_{BA}/RT]. \quad (4)$$

We have verified this form, with the overall preexponential factor proportional to $T$, for CO binding to the separated β-chain of hemoglobin Zürich [28]. $T_0$ is an arbitrary reference temperature which we take to be 100 K. The parameter $A_{BA}$ consequently gives the preexponential factor at 100 K. We further assume $g(H_{BA})$ to be given by the gamma distribution as in the model of Young and Bowne [29]. This distribution peaks at the activation enthalpy $H_{peak}$. The rebinding parameters are found by fitting the experimental data to eq. 3, with $g(H_{BA})$ given by the gamma distribution and $k_{BA}$ by eq. 4. We have used this technique for many heme protein-ligand systems [5,28,30]. The barrier parameters for binding to the A substates are given in table 2. For comparison, we also list the parameters obtained by monitoring at 440 nm.

### 3.4. The B substates

Since we observe four discrete CO-bound substates, $A_0$–$A_3$, we also expect four discrete sub-

Table 2
Barrier parameters for CO binding to A substates

| Substate | $H_{peak}$ (kJ/mol) | $\log[A_{BA}$ (100 K)/$s^{-1}]$ |
|---|---|---|
| $A_0$ | 10 | 10.8 |
| $A_1$ | 9.5 | 9.3 |
| $A_3$ | 18 | 9.8 |
| Soret (440 nm) | 10.1 | 9.0 |

states in the photodissociated state B. We observe, however, only three bands as shown in fig. 1b. In an earlier paper [8] we have discussed these bands in detail. $B_2$ at 2119 $cm^{-1}$ is an intermediate that decays to $B_1$ at temperatures above 15 K. For the treatment of rebinding above about 15 K, we are left with only $B_0$ and $B_1$. At pH 5.6 and 6.8, band $B_1$ is much more intense than $B_0$ and decays with the same time dependence as $A_1$ increases, while $B_0$ shows the same time dependence as $A_3$. $B_1$ therefore must bind to substate $A_1$ and $B_0$ to substate $A_3$.

The fact that we cannot see the B substates that bind to $A_0$ and $A_2$ is not surprising. The integrated extinction coefficients of the B bands are small ($1.4 \pm 0.1$ $mM^{-1}$ $cm^{-2}$) and a sufficiently sensitive measurement of the spectrum is difficult. Moreover, the intensities of $A_0$ and $A_2$ are much smaller than that of $A_1$. We consequently expect the B substates that bind to $A_0$ and $A_2$ to be much smaller than $B_1$ and therefore to be hidden.

### 3.5. Rebinding observed between 350 and 800 nm

The different kinetics for the various A substates raises the question of whether similar differences can also be seen over the interval 350–800 nm, where the spectral features are dominated by the heme group. The time range from 100 ns to 300 s was scanned with our flash photolysis system at the wavelengths indicated in fig. 1a. Times from 60 s to about 30 ks were monitored with the OLIS-Cary spectrometer where the entire wavelength region was scanned. While small differences were observed, no major variations in the time course as a function of wavelength were found at pH 6.8. The fastest rebinding was observed around the maximum of the CO-bound spectrum, the slowest around the peak of deoxymyoglobin. The average rates at 421 and 440 nm differ by a factor of 2.2 at 60 K and 1.6 at 80 K. The kinetics at 440 nm, where we normally monitor rebinding, agrees well with that of the integrated A substates. The result is reassuring. Observations in the Soret region yield information about the average rebinding behavior.

### 3.6. Transitions among A substates?

We have shown in section 3.1 that the A substates are frozen when the protein is embedded in a solid matrix. This observation leaves open the possibility that even below 180 K transitions among B substates can take place. Transitions among the A substates could then be induced by light, for instance, through the chain $A_i \rightarrow B_j \leftrightarrow B_k \rightarrow A_l$. To study this possibility, we have performed a number of additional experiments.

#### 3.6.1. MbCO after illumination

If transitions among the B substates occur the ratios $A_i/A_1$ measured after cooling in the dark and after illumination should in general differ below 180 K. We have performed such experiments at 160, 140 and 120 K. The relative change in intensities after illumination is less than 1% for $A_1$ and less than 5% for $A_0$ and $A_3$. The B substates do not exchange significantly with each other below 180 K.

#### 3.6.2. Rebinding under illumination

As a second test, we measured the infrared spectrum as a function of time during exposure of the MbCO sample to constant illumination. Under the assumption that each A substate communicates only with one B substate and that neither A nor B substates exchange with each other, the rate $A \rightarrow B$, denoted by $k_L$, is determined by the intensity of illumination. Rebinding $B \rightarrow A$ is characterized by the rate $k$. The absorbance change $\Delta A_i(t)$ in the band $A_i$ is then given by

$$\Delta A_i(t) = \Delta A_i \{k_L/(k_L + k)\} \times \{1 - \exp[-(k_L + k)t]\}, \quad (5)$$

where $\Delta A_i$ is the maximum absorbance change of band $A_i$, corresponding to complete photodissociation. If the rebinding rate $k$ is given by a distribution, eq. 5 must be generalized.

For $k_L \gg k$, eq. 5, predicts two features: (a) The approach to the steady state at $t = \infty$ is given by $k_L$. (b) The steady-state value of the absorbance change, $\Delta A_i(\infty)$, is equal to $\Delta A_i$. At 40 K both of these predictions are correct to within about 3%. All A and B bands approach the steady

state with the same kinetics, given by $k_L$ and the steady-state values agree with the values shown in fig. 2. This result verifies that no transitions $A_i \leftrightarrow A_j$ or $B_i \leftrightarrow B_j$ take place at 40 K. Data at 60 K give the same result. At 70 K and above, however, $A_1$ approaches equilibrium much slower than predicted by eq. 5. The data can be explained if a small fraction of the $A_1$ substates are pumped into longer-lived states. Observations of all A and B substates rule out transitions from $A_1$ to other A substates. We discuss an explanation of the observed effect in section 4.5.

### 3.6.3. *Multiple-flash experiments*

As a third test, we have performed multiple-flash experiments at various temperatures. In these experiments [5,13,14], photodissociation is repeated before all Mb molecules have rebound a ligand. Monitoring of the separate A bands can reveal if pumping from one A substate to another occurs. At 40 K, flashes were repeated every 3000 s. No pumping from one A substate to another is observed over the course of four flashes.

### 3.6.4. *Photodissociation after illumination*

In the earlier multiple-flash experiments (monitored in the visible range), flashing is repeated on the order of 20 times at intervals of length $\tau$ [5]. If transitions from one substate to a longer-lived one occurred with a small probability, say $10^{-3}$, or only at times longer than $\tau$, they would not be detected. A different experiment permits the search for such rare transitions: We expose the sample to an intense white light ($k_L \approx 10\ s^{-1}$) for a time $t_L$ varying between 10 and $10^3$ s. The light continuously rephotolyzes the rebound CO. At 80 K and above more than 50% of the CO molecules rebind within less than 0.1 s and will therefore be rephotolyzed between $10^2$ and $10^4$ times. At the end of the illumination, the sample is completely photolyzed by a laser pulse and rebinding is measured. The results of such experiments at 30, 40, 92 and 139 K are given in fig. 16. At 30 K, a very small increase in long-lived states is seen for $t_L = 1100$ s.

At 40 K, pumping is still small. At higher temperatures, rebinding at short times remains unaltered; at 139 K, more than 90% of the photolyzed CO rebind without change in rate. The

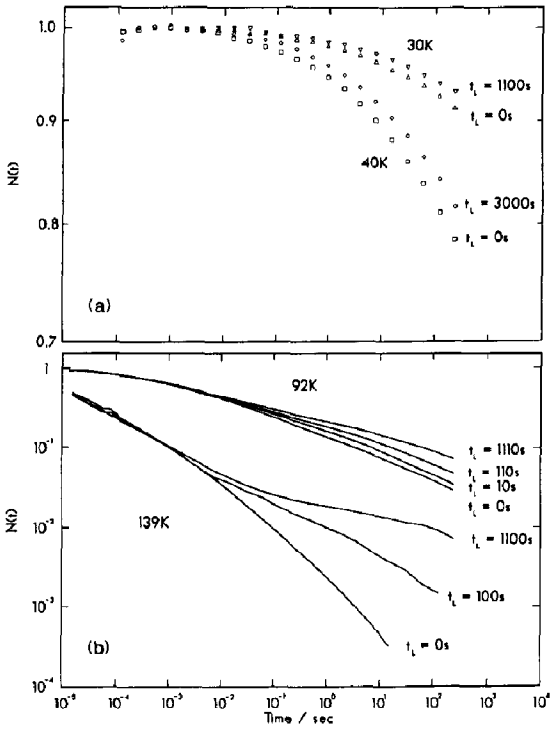


Fig. 16. Rebinding after illumination. The MbCO sample is illuminated by an intense white light for time $t_L$ before being photodissociated by a laser flash. Note the expanded scale for the absorbance change in (a). In (b) the lines have been drawn through each data point. Marker symbols have been omitted to avoid clutter.

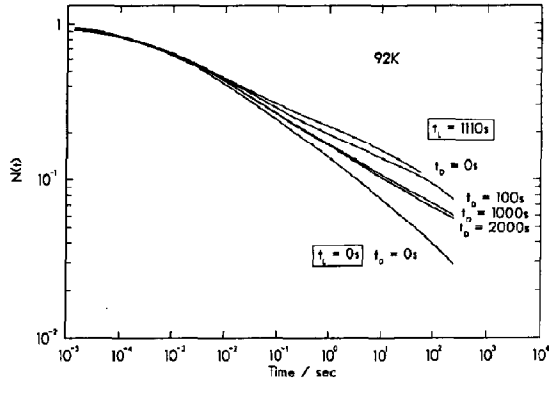


Fig. 17. Photodissociation after a delay $t_D$ following illumination for $t_L = 1110$ s. Normal 92 K rebinding kinetics ($t_L = 0$, $t_D = 0$) is included for comparison. Lines have been drawn through each data point. Solvent: 75% glycerol/water, pH 7.0.

change in the rebinding curve at long times, however, is dramatic; long-lived substates are greatly enhanced.

In a second set of experiments, a second laser pulse was applied with a delay, $t_D$, after the end of the illumination. The data at 92 K, shown in fig. 17, prove that the protein relaxes toward the initial state after the illumination is terminated. The relaxation is slow, however, and is not finished at time $t_D = t_L$. We interpret these results in terms of a hierarchy of substates in section 4.5.

## 4. Summary and interpretation

The experiments reported in section 3 answer the main questions raised in section 1, but also reveal new problems and point to new avenues of investigation. We summarize here the main results and interpret some of the new data.

### *4.1. Conformational substates*

One of the motivations for the present work was the question raised by the work of B. Chance et al. [15]: Is rebinding bi- or triphasic as originally claimed by Iizuka et al. [31] or is it characterized by a power law [5]? The result of the present work, displayed in figs. 14 and 15, is unambiguous: Regardless of where rebinding is monitored, the kinetics is smooth and nonexponential over more than 12 orders of magnitude in time. The original reason for introducing the concept of conformational substates is consequently still valid.

The observation of pumping into long-lived states (figs. 16 and 17) raises, however, the question of whether the arguments rejecting all models with only sequential [32] rather than parallel barriers are still valid. The answer is yes. The multiple-flash technique, described in detail elsewhere [13,14,33], is very sensitive to the difference between homogeneous and inhomogeneous systems and shows that the main components of the system must be inhomogeneous. We show in section 4.5.4. that the pumping experiments lead to a generalization of our model which can explain all data.

### *4.2. The substates in the heme pocket*

#### *4.2.1. The A substates*

It has been known for a considerable time that CO binds to the heme iron in more than one conformation [22,23,27,34]. Indeed, fig 5 shows four different stretching bands and implies four substates, $A_0$–$A_3$. The reversible exchange among the substates down to about 180 K, shown in fig. 6, implies that all bands correspond to folded, undenatured proteins and can occur within the same molecule. The main properties of the A substates are given in table 1 and figs. 6–9.

The spectroscopic data in section 3 together with the X-ray structure obtained at 260 K by Kuriyan et al. [35] permit a tentative structural assignment of $A_0$–$A_3$. Kuriyan et al. find four different orientations ('conformations A, B, C, D') of the bound CO molecule with respect to the heme groups and they refine two of the four. Their conformation C has an occupation of 78% and can therefore be identified with our substate $A_1$ which has an occupation of 70% at about pH 6 and 260 K. With this identification, $A_1$ has an angle $\theta$(Fe-C-O) of 141° and points toward C1D, the carbon atom 1 of pyrrole D of the heme group (the nomenclature is defined in fig. 2 of ref. 35). Their conformation D has an occupation of 22%. Fig. 5 shows that $A_3$ has a fractional intensity of about 25%. We therefore identify D with $A_3$. $A_3$ then has an angle $\theta = 120°$ and points in the direction of C4B, a considerable distance away from $A_1$.

We identify $A_0$ and at the same time solve an old problem by considering the effect of pH on $A_0$. Watson and Kendrew [36] pointed out that a water molecule bound to the iron in metMb would be within hydrogen-bonding distance of the distal His 64(E7). Since CO is not very different from a water molecule in size, a hydrogen bond between the oxygen of the CO and His E7 could be expected. Neutron diffraction data obtained by Hanson and Schoenborn [37], however, show no hydrogen bond in MbCO. If $A_0$ is identified with conformation A of Kuriyan et al., the following picture emerges: Of the four substates, $A_0$ is closest to His E7 and can form a hydrogen bond with $N^\epsilon$ if His E7 is protonated. If His E7 is the heme-linked protonation group with p$K$ = 5.7 ob-

served in optical and NMR measurements [38,39] we expect CO in the substate $A_0$ to be fully hydrogen-bonded to His E7 well below pH 5.7 and the hydrogen bond to be absent well above pH 5.7. The data in table 1 and fig. 9 support this expectation. At pH 5, substate $A_0$ is more tightly bound than $A_1$ by about 8 kJ/mol, and at pH 6.8 by about 4 kJ/mol. The difference, 4 kJ/mol, is consistent with a weak hydrogen bond. Additional evidence for the identification of $A_0$ comes from the angle $\theta = 154°$ for conformation A which is similar to the angle found in chelated protoheme-CO [40]. Heme carbonyls typically [41] have CO stretching frequencies near 1970 $cm^{-1}$, similar to the value for $A_0$. The fact that no hydrogen bond is seen in the neutron diffraction data is explained by the low intensity of substate $A_0$ at room temperature and the absence of protonated His E7 near neutral pH. To test the assignments directly, the intensities of the infrared bands and the X-ray conformations should be measured on the same crystal at a pH for which $A_0$ is sufficiently populated. Moreover, additional pH studies are needed to determine whether the four bands correspond to four distinct orientations or two bands correspond to the protonated and deprotonated forms of a single orientation.

We summarize the complete assignment in table 3 where we also include the van der Waals energies calculated by Kuriyan et al. [35]. Table 3 shows that the calculated binding energies are close to the relative enthalpies found here but are generally larger. In reality, the difference in occupation is determined as much by the relative entropies as by the binding enthalpies.

Table 3

The values for $\nu_{CO}$ refer to a 75% glycerol/water solvent, pH 6.8 and 240 K. The conformation and their properties are from ref. 35, at 260 K and pH 6. $\phi$ and $\theta$ characterize the CO conformation; $\phi$, dihedral angle between the Fe-C-O and Fe-C-NC planes; $\theta$, the angle Fe-C-O [35].

| Substate | $\nu_{CO}$ ($cm^{-1}$) | $H_A$ (kJ/mol) | Conformation | $E_{vdW}$ [35] (kJ/mol) | $\phi$ (°) | $\theta$ (°) |
|---|---|---|---|---|---|---|
| $A_0$ | 1966 | −4 | A | −12 | 20 | 154 |
| $A_1$ | 1945 | 0 | C | −12 | 60 | 141 |
| $A_2$ | 1941 | – | (B) | +25 | 93 | 120 |
| $A_3$ | 1930 | 2 | D | +4 | −62 | 120 |

#### 4.2.2. Interpretation of the B substates

The infrared spectrum of the CO stretching modes in the photodissociated state B is shown in fig. 1b. Above 20 K only two bands, $B_0$ and $B_1$, are unambiguously observed. $B_0$ binds to substate $A_3$ and $B_1$ to $A_1$. At present, no X-ray diffraction data are available on the photodissociated CO, so no steric interpretation of the B substates can be given. The fact that no exchange among $B_0$ and $B_1$ is observed below about 180 K suggests that each is sterically close to the corresponding A substate.

### 4.3. CO binding at low temperature

#### 4.3.1. Binding pathways

Each Mb molecule possesses four different pathways within the pocket for CO binding. In 75% glycerol/water, there is no exchange among the four channels below about 170 K; above 180 K transitions $A_i \rightarrow A_j$ and presumably $B_i \rightarrow B_j$ occur. The kinetics of each of the four pathways is nonexponential in time below about 180 K, as shown in figs. 14 and 15. Each is governed by different barrier parameters as given in table 2.

The data provide no evidence for discrete waystations or 'docking' within the heme pocket as postulated by B. Chance et al. [42]. The substate $B_2$ decays quickly to $B_1$ at 20 K and above [8], long before any appreciable rebinding occurs. $B_1$ binds to substate $A_1$ with essentially the same kinetics as observed in the visible range. Above 20 K, no intermediate substates appear in either the bound or photodissociated CO bands.

#### 4.3.2. Reaction theory

The data in table 2 imply that both entropic and enthalpic factors control the binding reaction at the heme iron. $A_0$ and $A_1$ both have about the same peak activation enthalpy $H_{peak}$; the faster binding rate of $A_0$ relative to $A_1$ is caused by the larger preexponential factor, $A_{BA}$. $A_3$ has a slightly larger preexponential than $A_1$, but has a slower binding rate owing to a much larger peak activation enthalpy. An explanation of these characteristics in terms of the pocket structure and of specific residues will require detailed studies of binding rates as a function of pH and with modified myoglobins.

The parameters listed in tables 1 and 2 show a Brønsted correlation [43]: the most tightly bound substate, $A_0$, binds fastest; the most weakly bound, $A_3$, binds slowest. The same correlation is found for different heme proteins where the one with the most tightly bound ligand has the smallest activation enthalpy barrier [44]. Such a correlation is expected for an 'overcoupled' transition, where an increase in the well depth for the covalently bound state A leads to a decrease in the barrier between the pocket state B and A. The experimental result consequently demonstrates that CO binding to many heme proteins, in particular Mb, is overcoupled and not 'undercoupled' [45].

### 4.4. Influence of the environment and control

From the biological point of view, the most important feature of our data is the exquisite sensitivity of the occupation of the substates in the pocket to external parameters such as pH (fig. 12), pressure (fig. 11) and solvent state (figs. 2–4) [22,27]. Previously, we found that the association rate of CO to Mb increases with decreasing pH and follows a Henderson-Hasselbalch equation with $pK = 5.7$ [46]. The present data provide more insight into the pH dependence; a change in pH not only can affect the kinetics of an individual pathway, but also can shift the system from one pathway to another. Such shifts also occur on changes in pressure and solvent state. Three conclusions may be drawn from these experiments: (i) Processes in the heme pocket are extremely responsive to external influences. (ii) Infrared observation of ligand binding is a tool well suited for the investigation of the effect of external parameters. (iii) The sensitivity of the processes in the heme pocket to external parameters may be used in vivo for the control of protein reactions, for example, in membrane proteins through changes in membrane viscosity and composition, and in hemoglobin through quaternary changes. In all processes, entropy may play a more important role than enthalpy, as is suggested by table 2.

### 4.5. Protein dynamics and models

The sensitivity of the infrared stretching bands to the conformation of the protein makes them excellent probes for investigating protein dynamics and models. We sketch the background for such investigations and describe the conclusions that emerge from the experiments reported in section 3.

#### 4.5.1. The hierarchy of conformational substates

A model with a single set of CS is not capable of explaining all experiments. On the one hand, rebinding in a 75% glycerol/water solvent is nonexponential up to at least 170 K [28], and pressure titration experiments prove that transitions among the CS responsible for the nonexponential kinetics occur only above about 180 K [47]. On the other hand, evidence for slow transitions among substates even at 80 K comes from X-ray diffraction: The Debye-Waller factor of many atoms changes appreciably down to 80 K [48,49]. Studies of the rearrangement of the protein structure after photodissociation ('proteinquake') demonstrate that a hierarchy of motions exists and that protein conformations can be classified into a hierarchy of substates [17,50]. We depict in fig. 18 the hierarchy of CS as modified by the results of the present work.

Fig. 18 represents the conformational energy of MbCO drawn for various tiers as a function of a conformational coordinate (cc). The energy valley in the top diagram represents MbCO. The observation of four CO stretching bands implies that MbCO can exist in four distinct substates of the zeroth tier ($CS^0$), $A_0$–$A_3$. The nonexponential rebinding kinetics observed for each band suggests that the actual energy surface for each $CS^0$ consists of a large number of conformational substates of the first tier, $CS^1$. Each of these again is subdivided into a large number of substates of the second tier, $CS^2$. The furcation continues, but the lower tiers are not relevant for the present discussion.

At rest, a protein will not remain in one CS, but equilibrium fluctuations (EF) will move the protein from CS to CS. The rates of the EF depend strongly on temperature and environment. In 75% glycerol/water, only EF2 (and EF3...) take place below about 170 K, but each protein remains frozen in a particular $CS^1$. Above about 180 K, EF1 occur and the protein fluctuates

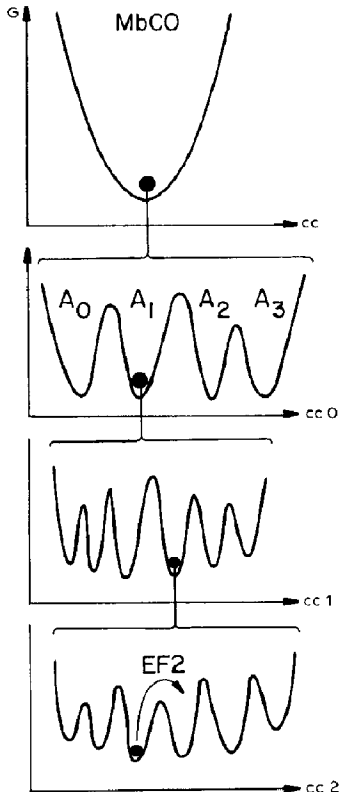


Fig. 18. Hierarchical arrangement of conformational substates (CS) in Mb. The conformational energy $G$ is drawn as a function of a conformational coordinate. The two lowest tiers, $CS^3$ and $CS^4$, have been omitted.

rapidly from one $CS^1$ to another. After photodissociation of MbCO, proteins relax from one state (MbCO) to another (Mb) through a sequence of functionally important motions (fims) [17].

*4.5.2. Relaxation of the A substates*

In a 75% glycerol/water solvent, the behavior of the A substates undergoes a change near 180 K. Below about 180 K the $CS^0$ no longer interconvert (fig. 6), the band frequency $\nu_{CO}$ stops shifting and the linewidth behavior changes. We interpret these features in terms of the $CS^1$. If the large-scale motions of the proteins are absent, the controlling side chains within the pocket may be prevented from fluctuating, thereby stopping transitions among the $CS^0$. This explanation also accounts for the large change in the linewidth $\Gamma$ of band $A_0$ in fig. 9. At pH 5 almost all of the His E7 are protonated and therefore most of the CO in state $A_0$ are hydrogen bonded. Below about 180 K, the motion of His E7 and therefore also that of CO is restricted, leading to a narrow band. Above 180 K, the side chain motion may also force the CO to large excursions, leading to a large $\Gamma$. Moreover, the probability of the hydrogen bond breaking increases with temperature, also leading to an increased linewidth.

*4.5.3. Slaved glass transition*

Mb in 75% glycerol/water possesses a remarkable transition between about 180 and 200 K as discussed in section 4.5.2. The transition occurs in an interval of about 20 K (figs. 6 and 8) and approach to equilibrium is nonexponential in time (fig. 10). These characteristics are similar to those observed in glass and spin glass transitions. Glasses (amorphous solids) [51–53] and spin glasses [54] are disordered and frustrated [55] systems that are believed to have a highly degenerate (many-valley) ground state [56]. The transition to the glass or spin glass state occurs in a finite temperature range and is nonexponential in time [57,58]. Because proteins are disordered and most likely frustrated systems [18] with many energy valleys (fig. 18) we expect a transition similar to a glass or spin-glass transition. The transition near 180 K satisfies all the requirements.

This transition manifests one property not encountered in glasses: It depends crucially on the solvent surrounding the protein. In 75% glycerol/water, the transition is at approx. 180 K (fig. 8). The solvent undergoes a glass transition at essentially the same temperature (fig. 13) [59,60]. In water, the transition is near 260 K, close to the melting point of the buffered solvent (fig. 6). In solid PVA, no transition in MbCO is apparent up to at least 300 K, although the ratio $A_3/A_1$ decreases gradually above 100 K. The observations imply that the EF1, the fluctuations of the $CS^1$, are suppressed when the protein environment is frozen or solid. The motions of the first tier thus are 'slaved' to the motions of the solvent and we consequently call the transition a 'slaved glass transition.'

The slaved glass transition is not a property of

the protein alone; protein and solvent together must be considered as one system. The hydration shell of the protein most likely plays a crucial role both in the glass transition and in the function of the protein [27,61,62]. Studies of the hydration water in Mb solutions and crystals by calorimetry and infrared spectroscopy show a broad glass transition between 180 and 270 K which depends on the degree of hydration [63].

*4.5.4. Pumping and substate symmetry breaking*

The results in figs. 16 and 17 appear at first to call for a new explanation of the nonexponential kinetics. We show here, however, that an extension of our earlier model explains the pumping into long-lived states. In that model [5] we ascribe the nonexponential kinetics to a distribution of activation enthalpies, characterized by the probability density $g(H_{BA})$ as given for the binding of CO to Mb in fig. 19a. Each substate $CS^1$ of the first tier in fig. 18 is characterized by a unique $H_{BA}$. Different $CS^1$ thus have different properties: the energy valleys of the first tier are not identical and we call this property 'substate symmetry breaking'. At this level of substate symmetry breaking the substates of the second tier, $CS^2$, have no effect on the activation energy for covalent bond formation. Experiments suggest that this assumption may be incorrect. The nonexponential relaxation in tier 2 seen in the proteinquake experiment [17] and the temperature dependence of the Debye-Waller factor below 180 K [48,49] imply that different $CS^2$ have different physical properties. The substate symmetry is thus also broken in the second tier, and we assume that different $CS^2$ have different barriers for the binding step $B \rightarrow A$. The $CS^1$ determine the barrier crudely, while the $CS^2$ fine-tune the barrier. We represent the situation in fig. 19b. Within each CS1, the CS2 determine a range of activation enthalpies. The distribution of barriers within a given $CS^1$ is indicated by the solid curves, and the overall distribution as determined by the $CS^1$ is given by the dashed envelope.

A possible explanation of the pumping observed in figs. 16 and 17 is now straightforward.

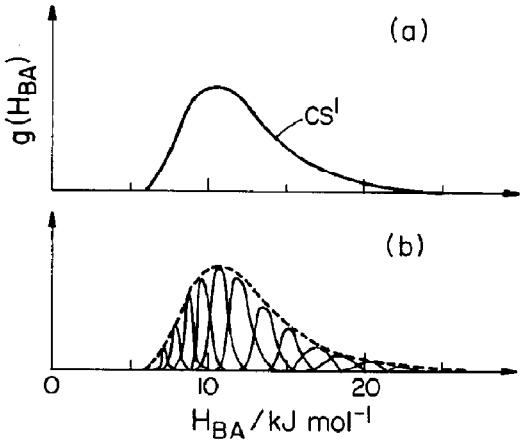


Fig. 19. (a) Activation enthalpy distribution $g(H_{BA})$ determined entirely by conformational substates of the first tier. (b) The overall distribution (dashed envelope) is determined by the substates of the first tier; the substates of the second tier provide the fine-tuning represented by the narrow solid distributions.

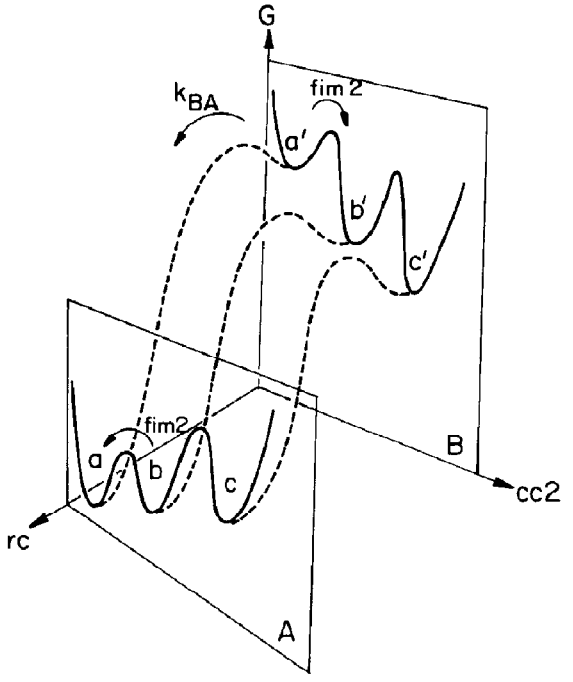


Fig. 20. Rebinding within one conformational substate of the first tier. The diagram shows the energy surfaces as a function of the conformational coordinate cc2 and the reaction coordinate rc. Details are given in the text.

Since the $CS^1$ are frozen below 180 K, we only have to consider a given $CS^1$. Fig. 20 gives a schematic representation of the barriers for the binding step B → A as a function of a conformational coordinate cc2 of the second tier. The two coordinates have very different meanings. The conformational coordinate cc2 describes the protein structure within a given $CS^1$; shown are three substates of the second tier, labelled a–c. The reaction coordinate rc describes the transition of the CO from the pocket (B) to the covalently bound state at the iron (A). The potentials along the reaction coordinate for fixed cc2 are drawn as dashed lines. If the system is initially in a, the lowest $CS^2$, photodissociation will move it to a′. The system can now either rebind, B → A, without change in cc2, or it can relax to another $CS^2$ of lower Gibbs energy, for instance, b′. We have studied the relaxation to lower $CS^2$ through fim 2 in detail and have found that it is nonexponential in time and extends over extremely large ranges in time [17]. In states b′ and c′, the barrier B → A may be either higher or lower than in a′. If it is lower, the system will rapidly return to b and from there relax to a. If it is higher, the system will stay longer in B and this behavior appears as pumping. The shift to longer rebinding times is caused by a relaxation in the protein coordinate [64] and not by a longer-lived intermediate state between B and A. The model explains both the pumping seen in fig. 16 and the relaxation in fig. 17. Relaxation occurs if the system is first pumped into long-lived $CS^2$, some of which rebind in the dark from, say, c′ to c. From there it will relax toward a, the lowest $CS^2$. A flash at a later time explores the degree of relaxation.

A theory of pumping remains to be constructed, but simple estimates indicate that the relaxation times and enthalpies observed are consistent with our earlier experiments [17]. Consider the pumping observed at 30 K in fig. 16. The absorbance scale is greatly expanded. The rate at $N(t) = 0.95$ changes by a factor of 2 after illumination for 1100 s. This rate change corresponds to a shift of $\delta H_{BA} \approx RT \ln 2 \approx 0.17$ kJ/mol. Since $g(H_{BA})$ extends from 5 to 25 kJ/mol, such a small shift is not even visible in fig. 19 and it is reasonable to attribute it to substates of the second tier. At 139 K, the largest time shift in fig. 16 corresponds to an enthalpy shift of $\delta H_{BA} \approx 8$ kJ/mol. This shift will change the distribution, but is still reasonable. Times and temperatures seen in pumping experiments are also consistent with fim 2 values. Recent measurements on fim 2 (unpublished data) indicate that it starts already at 30 K and extends to much longer times than those shown in ref. 17.

### 4.6. Remarks and outlook

#### 4.6.1. The infrared bands as tools

The experiments described and evaluated here demonstrate that infrared spectra, when studied as a function of time, temperature, solvent and pressure, provide a powerful tool for studies of protein dynamics and protein function. Nearly all investigations here mark a beginning, and extensions to shorter times, other systems, and other solvents are likely to yield even richer information.

#### 4.6.2. The Chance experiment

B. Chance et al. [15] have made two claims, that CO rebinding to Mb is bi- or triexponential at 40 K and that they can pump short-lived into long-lived states. Fig. 14 proves that the first claim is incorrect; data extended to $10^5$ s show no evidence for individual components. The second claim has to be discussed in more detail because of our new evidence for a small amount of pumping at 40 K in fig. 16. Chance et al. use a very weak pump light, adjusted so that on the average about 50% of the MbCO are photolyzed. Fig. 14 shows that $N(t)$ at 40 K drops 50% by about $5 \times 10^4$ s. Thus in their experiment, equilibrium can occur only for illumination times much greater than $5 \times 10^4$ s. Owing to the large distribution of flash-off rates $k_L$ through the thick sample, a time-dependent, nonequilibrium distribution of recombination rates is established in the sample. In the experiment of Chance et al., the relative amplitude of the slow components is enhanced by up to a factor of two, resulting in apparent pumping. Their result, therefore, can be explained without pumping in a straightforward way; it is caused by the combination of weak pump light, thick sample, nonexponential kinetics, and adjust-

ment to about 50% photolysis. A computer simulation of this combination, based on the generalization of eq. 5, reproduces the apparent pumping.

*4.6.3. Theories*

A goal of protein dynamics studies is a theory that classifies and describes protein states and protein motions. Remarkable progress toward this goal has been made with molecular dynamics computations, particularly by Karplus and collaborators [65]. Elber and Karplus [66] have verified the existence of multiple energy valleys with a 300 ps simulation. One unsolved question in such calculations concerns the level of substates that are reached. Comparison of the time scales simulated with those involved in the various tiers of substates [17] suggests that molecular dynamics explores many of the substates of tier 2, but cannot yet reach tier 1.

A second theoretical approach is based on ultrametricity [56]. We have proposed that the arrangement of the substates as shown in fig. 18 suggests ultrametricity [17]. Elber and Karplus have approached this problem with molecular dynamics [66] and find no evidence for ultrametricity. Since they investigate the distance matrix and we propose ultrametricity in the space of conformational energy, no disagreeement between the two models exists as yet. One possible problem regarding ultrametricity is raised by fig. 18: We have assigned the zeroth tier, $CS^0$, to the four A substates. Such an assignment is certainly correct below the glass temperature where no exchanges among the A substates take place. Above the glass temperature, however, both the $CS^0$ and $CS^1$ interchange, and it is no longer clear how to classify and order these substates. Additional investigations, both experimental and theoretical, may shed new light on these aspects of protein states and motions.

## Acknowledgements

We gratefully acknowledge the technical assistance of Stanley Luck and Rahul Pandharipande. Neil Alberding, Sam Bowne, Al Reynolds, and Erramilli Shyamsunder conducted some of the preliminary FTIR experiments. We thank Jim Alben, Anders Ehrenberg, Joel Friedman, John Kuriyan, Greg Petsko, Denis Rousseau, Benno Schoenborn, Ken Suslick and Peter Wolynes for illuminating discussions and advice. We thank Mary Ostendorf for her many efforts and technical assistance in manuscript preparation. R.D.Y. wishes to thank Illinois State University for research support. This work was supported in part by U.S. National Institute of Health grants GM 18051 and GM 32455, National Science Foundation grant DMB 82-09616, and Office of Naval Research grant N00014-86-K-00270.

## References

1 E. Antonini and M. Brunori, Hemoglobin and myoglobin in their reactions with ligands (North-Holland, Amsterdam, 1971).
2 R.H. Austin, K. Beeson, L. Eisenstein, H. Frauenfelder, I.C. Gunsalus and V.P. Marshall, Phys. Rev. Lett. 32 (1974) 403.
3 B. Chance, B. Schoener and T. Yonetani, in: Oxidases and related redox systems, eds T.E. King, H.S. Mason and M. Morrison (Wiley, New York, 1965) p. 609.
4 R.H. Austin, K. Beeson, L. Eisenstein, H. Frauenfelder, I.C. Gunsalus and V.P. Marshall, Science 181 (1973) 541.
5 R.H. Austin, K.W. Beeson, L. Eisenstein, H. Frauenfelder and I.C. Gunsalus, Biochemistry 14 (1975) 5355.
6 N. Alberding, R.H. Austin, K.W. Beeson, S.S. Chan, L. Eisenstein, H. Frauenfelder and T.M. Nordlund, Science 192 (1976) 1002.
7 J.O. Alben, D. Beece, S.F. Bowne, L. Eisenstein, H. Frauenfelder, D. Good, M.C. Marden, P.P. Moh, L. Reinisch, A.H. Reynolds and K.T. Yue, Phys. Rev. Lett. 44 (1980) 1157.
8 J.O. Alben, D. Beece, S.F. Bowne, W. Doster, L. Eisenstein, H. Frauenfelder, D. Good, J.D. McDonald, M.C. Marden, P.P. Moh, L. Reinisch, A.H. Reynolds, E. Shyamsunder and K.T. Yue, Proc. Natl. Acad. Sci. U.S.A. 79 (1982) 3744.
9 F.G. Fiamingo and J.O. Alben, Biochemistry 24 (1985) 7964.
10 L. Stryer, Biochemistry (Freeman and Co., San Francisco, 1981).
11 K. Gerwert, R. Rodriguez-Gonzalez and F. Siebert, in: Time-resolved vibrational spectroscopy, eds. A. Laubereau and M. Stockburger (Springer-Verlag, Berlin, 1985) p. 263.
12 M. Chance, B. Campbell and J. Friedman, Biophys. J. 51 (1987) 291a.
13 H. Frauenfelder, Methods Enzymol. 54 (1978) 506.
14 H. Frauenfelder, in: Structure and dynamics: nucleic acids and proteins, eds. E. Clementi and R.H. Sarma (Adenine, Guilderland, NY, 1983) p. 369.

15 B. Chance, L. Powers, Y.-H. Zhou and A. Naqui, Bull. Am. Phys. Soc. 31 (1986) 386; B. Chance, L. Powers, C. Zhou, A. Naqui and M. Chance, Biophys. J. 49 (1986) 537a; B. Chance, Y.-H. Zhou, K.S. Reddy and L. Powers, Fed. Proc. 45 (1986) 1641.
16 H. Frauenfelder, G.A. Petsko and D. Tsernoglou, Nature 280 (1979) 558.
17 A. Ansari, J. Berendzen, S.F. Bowne, H. Frauenfelder, I.E.T. Iben, T.B. Sauke, E. Shyamsunder and R.D. Young, Proc. Natl. Acad. Sci. U.S.A. 82 (1985) 5000.
18 D. Stein, Proc. Natl. Acad. Sci. U.S.A. 82 (1985) 3670.
19 A. Ansari, J. Berendzen, D. Braunstein, B.R. Cowen, H. Frauenfelder, M.K. Hong, I.E.T. Iben, P. Ormos, T.B. Sauke, A. Schulte, P.J. Steinbach and R.D. Young, Biophys. J. 51 (1987) 289a; two additional, related abstracts also appear in this issue of Biophys. J.
20 W.A. Eaton and J. Hofrichter, Methods Enzymol. 76 (1981) 175.
21 M.W. Makinen and A.K. Churg, in: Iron porphyrin, part 1, eds. A.B.P. Lever and H.B. Gray (Addison-Wesley, Reading, MA, 1982) p. 141.
22 M.W. Makinen, R.A. Houtchens, and W.S. Caughey, Proc. Natl. Acad. Sci. U.S.A. 76 (1979) 6042.
23 W. Caughey, H. Shimida, M.G. Choc and M.P. Tucker, Proc. Natl. Acad. Sci. U.S.A. 79 (1981) 2903.
24 B.L. Roberts, R.A.J. Riddle and G.T.A. Squier, Nuclear Instrum. Methods 130 (1975) 559.
25 C.J. Batty, S.D. Hoath and B.L. Roberts, Nuclear Instrum. Methods 137 (1976) 179.
26 L. Cordone, A. Cupane, M. Leone and E. Vitrano, Biophys. Chem. 24 (1986) 259.
27 W.E. Brown, III, J.W. Sutcliffe and P.D. Pulsinelli, Biochemistry 22 (1983) 2914.
28 D.D. Dlott, H. Frauenfelder, P. Langer, H. Roder and E.E. DiIorio, Proc. Natl. Acad. Sci. U.S.A. 80 (1983) 6239.
29 R.D. Young and S.F. Bowne, J. Chem. Phys. 81 (1984) 3730.
30 F. Stetzkowski, R. Banerjee, M.C. Marden, D.K. Beece, S.F. Bowne, W. Doster, L. Eisenstein, H. Frauenfelder, L. Reinisch, E. Shyamsunder and C. Jung, J. Biol. Chem. 260 (1985) 8803.
31 T. Iizuka, H. Yamamoto, M. Kotani and T. Yonetani, Biochim. Biophys. Acta 371 (1974) 126.
32 M. Marden, Eur. J. Biochem. 128 (1982) 399.
33 K.T. Yue, Ph.D. Thesis, University of Illinois at Urbana-Champaign, Urbana, IL (1983).
34 S. McCoy and W.S. Caughey, in: Probes of structure and function of macromolecules and membranes, vol. 2, eds. B. Chance, T. Yonetani and A.S. Mildvan (Academic Press, New York, 1971) p. 289.
35 J. Kuriyan, S. Wilz, M. Karplus and G.A. Petsko, J. Mol. Biol. 192 (1986) 133.
36 H.C. Watson and J.C. Kendrew, Nature 190 (1961) 670.
37 J.C. Hanson and B.P. Schoenborn, J. Mol. Biol. 153 (1981) 117.
38 Y. Hayashi, H. Yamada and I. Yamazuki, Biochim. Biophys. Acta 427 (1976) 608.
39 G.N. La Mar, D.L. Budd, H. Sick and K. Gersonde, Biochim. Biophys. Acta 537 (1978) 270.
40 A. Bianconi, A. Congiu-Castellano, M. Dell'Ariccia, A. Giovannelli, E. Burattini, P.J. Durham, G.M. Giacometti and S. Morante, Biochim. Biophys. Acta 831 (1985) 114.
41 J.O. Alben and W.S. Caughey, Biochemistry 7 (1968) 175.
42 L. Powers, B. Chance, A. Naqui, Y.-H. Zhou and M. Chance, Biophys. J. 51 (1987) 290a; B. Chance, Bull. Am. Phys. Soc. 32 (1987) 429.
43 L.I. Krishtalik, Charge transfer reactions in electrochemical and chemical processes (Consultants Bureau, New York, 1986).
44 N. Alberding, S.S. Chan, L. Eisenstein, H. Frauenfelder, D. Good, I.C. Gunsalus, T.M. Nordlund, M.F. Perutz, A.H. Reynolds and L.B. Sorensen, Biochemistry 27 (1978) 43.
45 R.F. Goldstein and W. Bialek, Comments Mol. Cell. Biophys. 3 (1986) 407.
46 W. Doster, D. Beece, S.F. Bowne, E.E. DiIorio, L. Eisenstein, H. Frauenfelder, L. Reinisch, E. Shyamsunder, K.H. Winterhalter and K.T. Yue, Biochemistry 21 (1982) 4831.
47 L. Eisenstein and H. Frauenfelder, in: Frontiers of biological energetics: Electrons to tissues, vol. 1, eds. L.P. Dutton, J.S. Leigh and A. Scarpa (Academic Press, New York, 1979) p. 680.
48 H. Hartmann, F. Parak, W. Steigemann, G.A. Petsko, D. Ringe Ponzi and H. Frauenfelder, Proc. Natl. Acad. Sci. U.S.A. 79 (1982) 4967.
49 F. Parak, H. Hartmann, K.D. Aumann, H. Reuscher, G. Rennekamp, H. Bartunik and W. Steigemann, J. Mol. Biol. (1987) in the press.
50 H. Frauenfelder and R.D. Young, Comments Mol. Cell. Biophys. 3 (1986) 347.
51 J.M. Ziman, Models of disorders (Cambridge University Press, Cambridge, 1979).
52 R. Zallen, The physics of amorphous solids (John Wiley, New York, 1983).
53 J. Jäckle, Rep. Prog. Phys. 49 (1986) 171.
54 K. Binder and A.P. Young, Rev. Mod. Phys. 58 (1986) 801.
55 G. Toulouse, Commun. Phys. 2 (1977) 115.
56 R. Rammal, G. Toulouse, and M.A. Virasoro, Rev. Mod. Phys. 58 (1986) 765.
57 G.W. Scherer, Relaxation in glass and composites (John Wiley, New York, 1986).
58 O. Beckman, Festkörperprobleme 25 (1985) 233.
59 R.L. Bohon and W.T. Conway, Thermochim. Acta 4 (1972) 321.
60 P.L. Kuhns and M.S. Conradi, J. Chem. Phys. 77 (1982) 1771.
61 V.I. Goldanskii and Yu.F. Krupyanskii, in: Proceedings of the international conference on the applications of the Mössbauer effect, vol. 1 (Gordon and Breach, New York, 1985) p. 83.
62 G.P. Singh, F. Parak, S. Hunklinger and K. Dransfeld, Phys. Rev. Lett. 47 (1981) 685.
63 W. Doster, A. Bachleitner, R. Dunau, M. Hiebl and E. Lüscher, Biophys. J. 50 (1986) 213.
64 N. Agmon and J.J. Hopfield, J. Chem. Phys. 78 (1983) 6947.
65 M. Karplus and J.A. McCammon, Annu. Rev. Biochem. 52 (1983) 263.
66 R. Elber and M. Karplus, Science 235 (1987) 318.